ELSEVIER

Spectrochimica Acta Part B 55 (2000) 279–297

SPECTROCHIMICA ACTA PART B

www.elsevier.nl/locate/sab

Behavior of the sputtered copper atoms, ions and excited species in a radio-frequency and direct current glow discharge

Annemie Bogaerts*, Renaat Gijbels

Department of Chemistry, Uni ersity of Antwerp (UIA), Uni ersiteitsplein 1, B-2610 Wilrijk-Antwerp, Belgium

Received 27 September 1999; accepted 17 December 1999

Abstract

The behavior of the sputtered copper atoms and ions, both in the ground state and in excited levels, is modeled with a collisional–radiative model and two Monte Carlo models. The models are applied to a glow discharge operated in either the direct current (dc) or the radio-frequency (rf) mode, at similar conditions of gas pressure and electrical power (i.e. 5 torr and approx. 38 W). Typical results of the model are the level populations of all copper atomic and ionic levels, the relative contributions of various populating and depopulating processes, as well as the optical emission intensities of copper atomic and ionic lines. These results will be presented and compared for both operation modes.

Keywords: Glow discharge; Direct current; Radio-frequency; Argon; Copper; Collisional–radiative model; Sputtering; Optical emission spectrometry

1. Introduction

In a previous paper [1] a model has been presented for the argon atoms in various excited levels in a glow discharge operated in the direct current (dc) and in the radio-frequency (rf) mode. Moreover, in recent years we have also developed a number of models for the electrons, argon ions (Ar^+, Ar_2^+ and Ar^{2+}), fast argon atoms, and sputtered copper atoms and ions in a dc glow discharge (see refs. [1–9] in Bogaerts and Gijbels [1]), and for the electrons, argon ions and fast argon atoms in an rf discharge (see refs. [10,11] in

* Corresponding author. Tel.: 32-3-820-2364; fax: 32-3-820-2376.
E-mail address: bogaerts@uia.ua.ac.be (A. Bogaerts)

0584-8547/00/$ - see front matter
PII: S0584-8547(00)00142-7

Bogaerts and Gijbels 1). In order to close the loop of the models and to obtain a complete picture of the rf discharge, the present paper therefore treats the model describing the copper species in the rf discharge. Moreover, a comparison will be made between the rf and dc discharges, at similar values of pressure and electrical power and, where possible, these comparisons will be checked with experimental observations.

2. Description of the model

The present model for the copper species fits in a global modeling network, consisting of Monte Carlo models, fluid models and collisional–radiative models to describe the behavior of electrons, argon ions, fast argon atoms, argon atoms in various excited levels, and copper atoms and ions, in order to obtain an overall picture of the argon glow discharge with copper cathode. More details about these models are given, e.g. in refs 1–9 of Bogaerts and Gijbels 1 , and will not be repeated here. The present paper deals only with the models describing the copper species.

Three different models treat different aspects of the copper species. The sputtering of copper atoms at the rf-electrode or cathode is calculated based on the flux energy distributions of the argon ions, fast argon atoms and copper ions (see below) at the electrode, multiplied with an empirical formula for the sputtering yield as a function of the bombarding energy (see e.g. 2). The atoms are sputtered with energies in the order of 5–10 eV. They lose this energy very rapidly by collisions with the argon gas atoms, until they are thermalized. Since this thermalization processes is considered to be very fast, it is assumed to be finished before the copper atoms can start to diffuse or become ionized or excited. Therefore, this process is separated in time from the further behavior of the copper atoms, and it is treated with a *Monte Carlo model* (for more information, see Bogaerts et al. 3). Output of this model is a so-called 'thermalization profile', i.e. the number of thermalized atoms as a function of position, which is used as input in the next model.

Once the copper atoms are thermalized, they start to move by diffusion. Moreover, they can become ionized or excited. This behavior of the copper atoms (diffusion, ionization, excitation), as well as the behavior of the created copper ions, and atoms and ions in excited levels, is described with a *collisional–radiati e model*. Eight copper atomic and seven copper ionic levels are considered in this model, as well as the Cu^{2} ions. Some of these levels are individual levels, whereas others are 'effective levels', i.e. a group of individual levels with similar excitation energy and quantum numbers. A schematic picture of the energy level scheme is presented in Fig. 1 4 . The levels taken into account in our model are depicted with black lines, and they are numbered with an effective level number, at the left side. The levels indicated in gray are not described in our model, because they have lower populations and do not give rise to intense lines in the optical emission spectrum, and or because the necessary cross sections to calculate their level populations are not available. More information about the levels taken into account (e.g. statistical weights and excitation energy) are presented in Bogaerts et al. 4 .

The populating and depopulating processes for the various levels taken into account in this model are the following collisional and radiative processes (this is where the characteristic name comes from):

1. Electron impact excitation and de-excitation between the levels (both for the copper atoms and ions).
2. Electron impact ionization from the Cu^{0} atoms to the Cu ions, and from the Cu ions to the Cu^{2} ions.
3. Three-body recombination where the third body is an electron, from the Cu^{2} ions to the highest Cu level, and from the Cu ions to the highest Cu^{0} level.
4. Electron impact ionization from the Cu^{0} atoms to the Cu^{2} ions.
5. Excitation and de-excitation between copper atom levels, due to collisions with argon gas atoms or copper ground state atoms (since

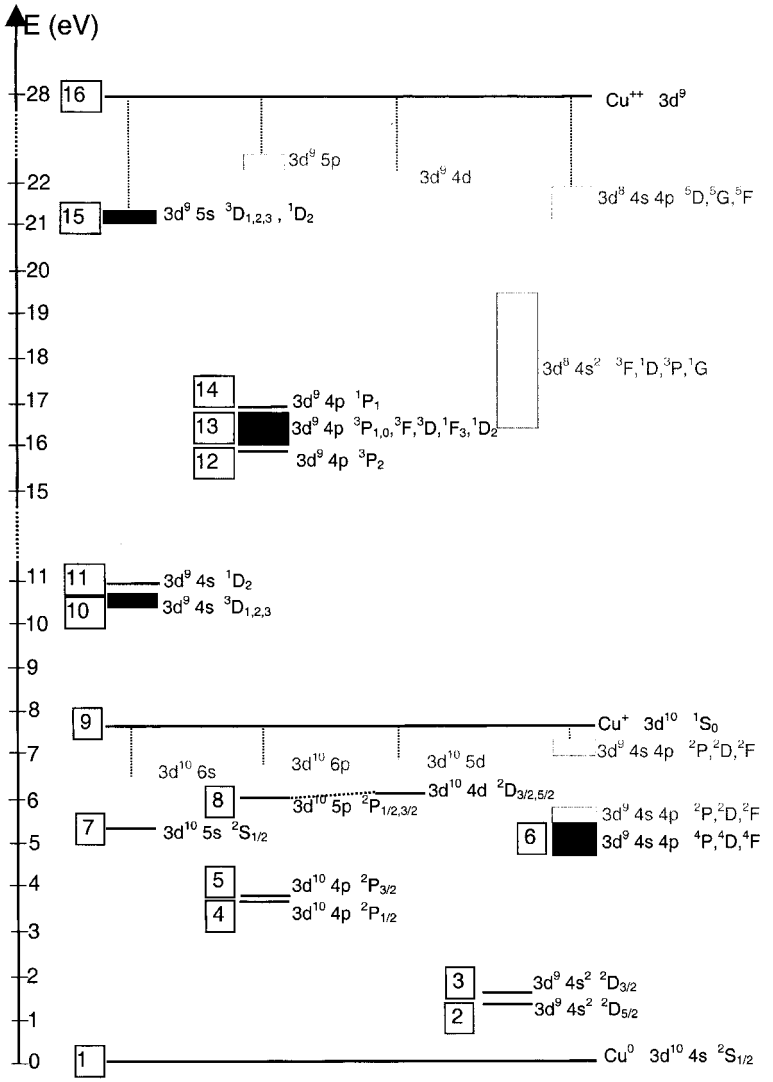

Fig. 1. Energy level scheme of the copper atoms and ions, with the effective level number (left) and the designation according to Moore (right of the levels). The levels drawn in black are taken into account in our model. Reprinted from Bogaerts et al. 4 with permission of Elsevier Science Inc.

the argon and copper atoms have thermal energy, excitation will only occur between two closely lying levels).

6. Penning ionization of copper atoms, due to collisions with argon metastable atoms.
7. Asymmetric charge transfer with argon ions (Cu^0 Ar $\rightarrow$ Cu Ar^0).
8. Radiative decay between all copper atomic and ionic levels. When this decay occurs to the copper atomic ground state, a fraction of the emitted radiation can be reabsorbed, so that only a small fraction, defined by the 'escape factor' can escape. More information about this 'radiation trapping' is given in Bogaerts et al. 4 . It should be mentioned that radiation trapping was found to be not important for transitions to other levels than the copper atomic ground state, due to their lower populations.
9. Finally, the most important production

process for the copper atoms in the ground state is the sputtering from the rf-electrode cathode. This production term is given as sputtering flux (calculated as the product of the flux energy distributions of the bombarding plasma species and an empirical formula for the sputtering yield as a function of bombarding energy, see above), multiplied with the thermalization profile (see above).

The level populations of the eight copper atomic and the seven Cu ionic levels, as well as the Cu^2 ions, are calculated with a set of balance equations, incorporating all the above mentioned populating and depopulating processes:

$$\frac{\partial n_{a\text{-}i}(z,r)}{\partial t} \quad \overline{\nabla}\cdot\overline{J_{a\text{-}i}}(z,r)$$

$$R_{\mathrm{pop},a\text{-}i}(z,r) \quad R_{\mathrm{depop},a\text{-}i}(z,r)$$

where $n_{a\text{-}i}$ and $J_{a\text{-}i}$ are the densities and fluxes of all atomic (a) and ionic (i) levels, and $R_{\mathrm{pop},a\text{-}i}$ and $R_{\mathrm{depop},a\text{-}i}$ comprise all populating and depopulating processes of levels a and i (see above), all as a function of axial (z) and radial (r) direction, in a cylindrically symmetrical glow discharge cell. Transport occurs by diffusion for the atomic levels, and by diffusion and migration for the ionic levels:

$$\overline{J_a}(z,r) \qquad D\overline{\nabla}n_a(z,r)$$

$$\overline{J_i}(z,r) \qquad D\overline{\nabla}n_i(z,r)$$

$$\mu n_i(z,r)\overline{\nabla}V(z,r)$$

where D and μ are the diffusion coefficient (the same for the atoms and ions) and mobility, respectively.

Since the populations of the various levels are affected by the populations of the other levels due to excitation, de-excitation, ionization, recombination and radiative decay processes, the 16 balance equations are coupled and solved simultaneously until convergence is reached. More information about this model (e.g. cross sections, transition probabilities, etc.) can be found in Bogaerts et al. 4 .

Finally, in order to calculate the flux energy distribution of the copper ions bombarding the rf-electrode cathode, which is necessary to calculate the sputtering flux (see above), the copper ions are also followed in the sheath adjacent to this electrode with a *Monte Carlo model*. The ions enter the sheath from the bulk plasma, determined by their flux, calculated in the above collisional–radiative model. Moreover, they can be created in the sheath due to ionization collisions, which is also calculated in the collisional–radiative model. On their way towards the rf-electrode cathode, they can collide with argon gas atoms, changing their energy and direction. However, in practice most of the copper ions will be directed towards the electrode by the electric field, and they will arrive at the electrode with rather high energy (see below).

The three models described above are coupled to each other and to the models describing the other plasma species, due to the interaction processes between the species, and they are solved iteratively until final convergence is reached. A flowchart of how the models are coupled is presented in Fig. 2.

3. Results and discussion

3.1. Cell geometry and discharge conditions

The cell geometry assumed in the model is a simple cylinder, with length equal to 2 cm and diameter equal to 4 mm. The rf-powered electrode or cathode (sample) is found at one end of the cylinder, whereas the other end of the cylinder, as well as the side walls, are grounded. This is a simplification of a Grimm-type geometry with anode diameter of 4 mm. Indeed, the Grimm cell is typically longer and becomes wider at longer distances from the sample. However, the plasma is most intense only in the first centimeters from the electrode. Hence, the cell geometry being studied is a good approximation of the real Grimm-type geometry.

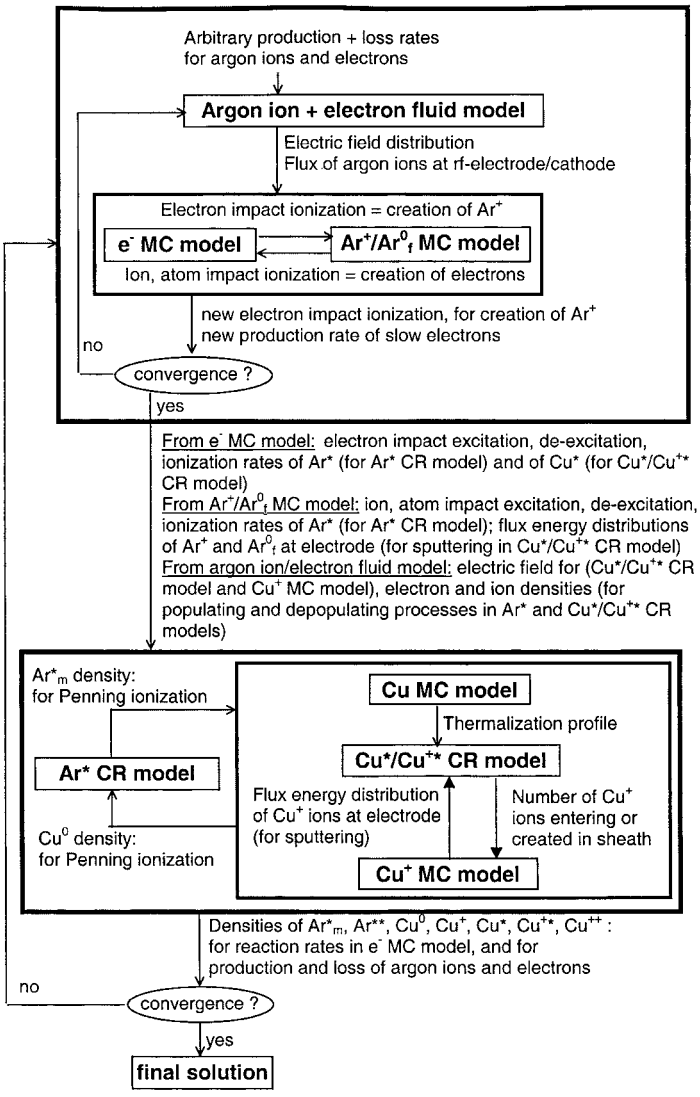

Fig. 2. Flowchart of the entire modeling network.

The discharge conditions under investigation are based on measurements by Hoffmann 5 for a Grimm-type cell with 4-mm anode diameter, i.e. an argon gas pressure of 5 torr and an electrical power in the order of 38 W, for both the rf and dc mode (more exactly 37 W for the rf, and 38 W for the dc mode). This corresponded, according to his measurements, to a dc voltage and current of 1000 V and 38 mA, and rf voltages of 680 V (rf-amplitude) and 569 V (dc-bias). In our model, we can calculate the electrical parameters in a self-consistent way, which is used as the primary check for validity of the model. In the dc case, we calculated, at a gas pressure of 5 torr, a gas temperature of 1100 K and a dc voltage of 1000 V (all used as input), an electrical current of 38.5 mA, and hence a power of 38.5 W, which is in excellent agreement with the experimental observations. In the rf model, the electrical power is used as input value. For a power of 37 W, and a

gas pressure and temperature of 5 torr and 1100 K, we calculated rf voltages of 769 V (rf-amplitude) and 519 V (dc-bias). Hence, the calculated rf-amplitude was somewhat too high, and the dc-bias was calculated a bit too low, but the values are still in the correct order of magnitude, and what is more important, lower voltages were predicted in the rf case than in the dc case, for the same power level. This is not a straightforward result, because in an earlier version of our rf-model, the opposite trend was predicted (see the discussion in Bogaerts et al. 6). Hence, we were already very satisfied with the present correlation between model and experiment, especially because the uncertainties in the modeling results may be considerable, e.g. due to some uncertainties in various input parameters such as cross sections. A picture illustrating the calculated and measured voltages in the rf case (as a function of time in the rf-cycle) and in the dc-case, as well as the electrical current and power, was presented in Bogaerts and Gijbels 1 .

Besides measuring the electrical parameters, Hoffmann also performed some measurements on the erosion rates and emission intensities for the above discharge conditions. He found that the erosion rate was approximately 1 μm in 8 s in the rf discharge, and slightly lower (i.e. 1 μm in 9 s) in the dc discharge. Also the emission intensities of analyte lines (of Si, Ni and Cu) were found to be approximately 10% lower in the dc discharge compared to the rf discharge. These data will be used later in this paper to check our modeling results.

3.2. Sputtering at the rf-electrode or cathode

As mentioned before, the sputtering flux is calculated based on the product of the sputtering yield as a function of the bombarding energy (calculated with an empirical formula) and the flux energy distributions of the argon ions, fast argon atoms and copper ions bombarding the rf-electrode or cathode. Complete flux energy distributions of these species in both the rf mode (as a function of time) and the dc mode are not presented here, but instead, the fluxes and mean energies of the three kinds of species are illustrated in Fig. 3, both in the rf and dc mode. For simplicity, the fluxes are given as positive values, but it should be mentioned that they are all directed towards the rf-electrode cathode. They are depicted with solid lines (left axis) whereas the dashed lines represent the mean energies (right axis). Moreover, the rf results (as a function of time) are shown with black curves, whereas the dc results (constant in time) are presented with gray lines. The rf Ar ion flux (Fig. 3a) is in the

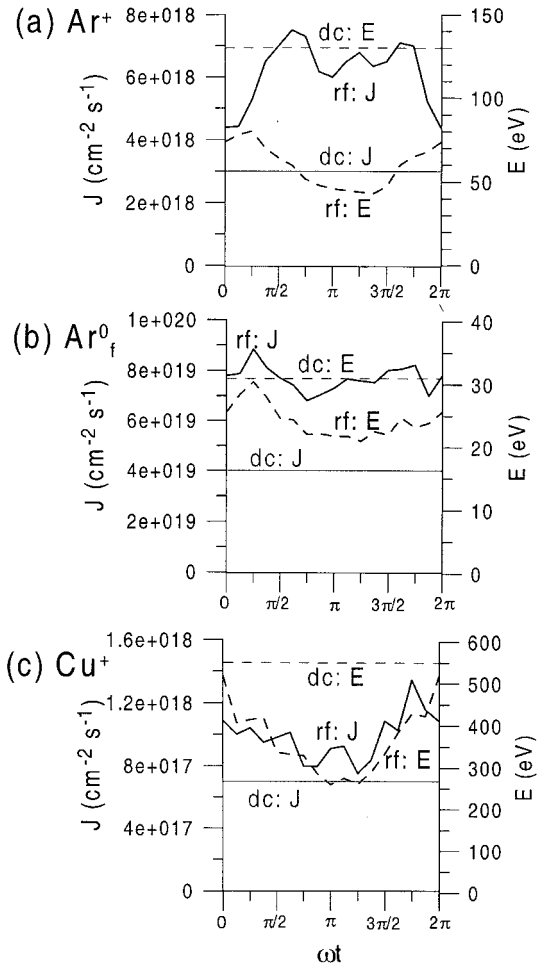

Fig. 3. Fluxes (solid lines; left axes) and mean energies (dashed lines; right axes) of the argon ions (a), fast argon atoms (b), and copper ions (c) bombarding the rf-electrode or cathode, in the rf and dc discharge, (black and gray curves, respectively), at the conditions of 5 torr, 37 W, 769 V (rf-amplitude) and 519 V (dc-bias) for the rf-case; and 38.5 W and 1000 V, for the dc case.

order of 4–8 10^{18} s ^{1}. It appears to reach a minimum around ωt 0 2π and a maximum around ωt π 2. The Ar ion energy in the rf mode varies between 40 eV around ωt π–3π 2 and 70 eV at approximately ωt 0 and slightly later. The dc ion flux appears to be slightly lower (i.e. approx. 3 10^{18} s ^{1}) but the ion energy is found to be higher (approx. 130 eV). This is like expected because, for the same power and pressure values, the dc discharge is characterized by a higher voltage (which gives rise to higher energies) and hence a lower current (yielding a lower ion flux).

A similar picture is also found for the fast Ar atoms (Ar_f^0; Fig. 3b) and the Cu ions (Fig. 3c). Indeed, the dc flux is typically somewhat lower and the dc mean energy somewhat higher than the corresponding rf values, i.e. for the Ar_f^0 atoms: J_{rf} 8 10^{19} s ^{1}; J_{dc} 4 10^{19} s ^{1}; E_{rf} 20–30 eV; E_{dc} 30 eV; and for the Cu ions: J_{rf} 8 10^{17}–1.2 10^{18} s ^{1}; J_{dc} 7 10^{17} s ^{1}; E_{rf} 250–500 eV; E_{dc} 550 eV. Looking at the time evolution in the rf case, it follows that the Ar_f^0 atoms reach more or less a maximum flux and energy between ωt 0 and π 2, and a minimum flux and energy around ωt π and between ωt π and 3π 2, respectively. Similarly, the flux and energy of the Cu ions both reach a maximum around ωt 0, and a minimum between ωt π and 3π 2. However, the time variations are in general rather small.

The sputtering yield of copper atoms, calculated with the empirical formula of Matsunami et al. 7 , is illustrated in Fig. 4, as a function of the bombarding energy of argon and copper species. It follows that the sputtering yield increases at higher energy, for the energy range of interest to us, with a threshold approximately 20 eV. Moreover, it is slightly higher for copper bombardment than for argon bombardment, due to the higher mass of the copper species.

Taking into account that (i) the sputtering efficiency increases at higher bombarding energy; (ii) the number of sputtered atoms is proportional to the number (and hence, the flux) of incoming particles; and (iii) the fast argon atoms are mainly responsible for the sputtering (see below), it is expected, based on Fig. 3, that the sputtering flux

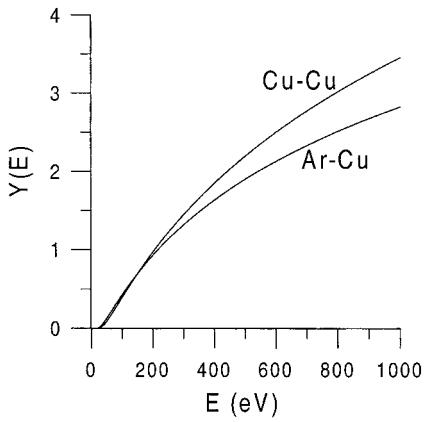

Fig. 4. Sputtering yield of copper atoms as a function of the bombarding energy for argon species bombardment and copper bombardment, calculated with the empirical formula of Matsunami et al. 7 .

is somewhat higher between ωt 0 and π 2, and reaches a minimum between ωt π and 2π. This is indeed illustrated in Fig. 5, which shows the calculated 'net' sputtering fluxes, as a function of time in the rf-cycle, for the rf discharge, and also for the dc discharge (constant in time). The sputtering flux is calculated to vary between 2 and 4 10^{17} s ^{1} (hence a variation of a factor of two) for the rf mode, and is in the order of 2 10^{17} s ^{1} for the dc discharge. The fact that the sputtering flux is calculated to be somewhat lower in the dc mode (for comparison: the time-averaged rf sputtering flux was found to be approx. 2.7 10^{17} s ^{1}) tells us that the lower flux plays a more important role in determining the amount of sputtering than the higher bombarding energy (see Fig. 3).

It should be mentioned that the 'net' sputtering flux is obtained from the sputtering flux minus the redeposition flux. Indeed, a large fraction (in the order of 60–70%, similar in both the dc and the rf mode) of the sputtered atoms will diffuse back towards the cathode and will be redeposited. Hence, it is the net sputtering flux which gives rise to the erosion rate, by 8 :

$$\text{ER} \quad J_{\text{sput,net}} \frac{M}{N_A \rho}$$

where ER is the erosion rate (in cm s ^{1}), $J_{\text{sput,net}}$

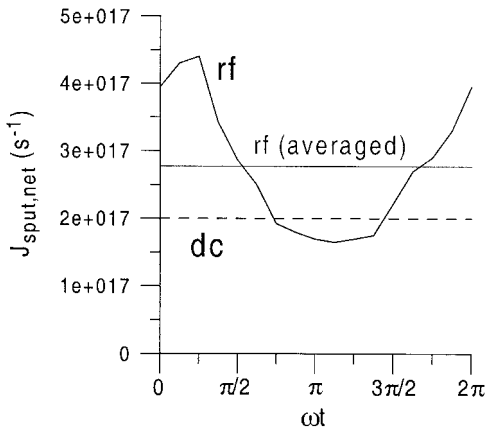

Fig. 5. Calculated net sputtering flux of the copper atoms, in the rf discharge (as a function of time in the rf-cycle: black solid line; as well as the time-averaged value: black dashed line) and in the dc discharge (constant in time; gray curve), for the same conditions as in Fig. 3.

is the net sputtering flux (in cm ^{2} s ^{1}), M and ρ are the atomic weight (in g mol ^{1}) and density of the sample material (ρ_{Cu} 8.92 g cm ^{3} 9), and N_A is Avogadro's number.

Averaged over time in the rf-cycle, the net sputtering flux is approximately 2.7 10^{17} s ^{1} (see Fig. 5) which means over the entire electrode area. For an anode diameter of 4 mm, the electrode area is approximately 0.126 cm^2. Hence, the net sputtering flux is approximately 2.1 10^{18} cm ^{2} s ^{1}, which corresponds to an erosion rate of approximately 0.253 μm s ^{1}. Experimentally, a value of 1μm in 8 s was measured 5 . Therefore, our calculated value (i.e. approx. 2.0 μm in 8 s) is a little bit higher, but still in the correct order of magnitude. In the dc case, the net sputtering flux, divided by the cathode area was approximately 1.6 10^{18} cm ^{2} s ^{1}. This corresponds to an erosion rate of approximately 0.19 μm s ^{1}. The experimental value was 1 μm in 9 s; hence our predicted value (i.e. approx. 1.7 μm in 9 s) is again slightly higher. It can be concluded that, although both calculated values are somewhat higher than the corresponding experimental data, the calculated relative difference between rf and dc erosion rates is in reasonable agreement with the experimental observations.

Finally, the relative contributions to the sputtering of the different plasma species bombarding the electrode are calculated. From the fluxes in Fig. 3 it could be deduced already that the fast

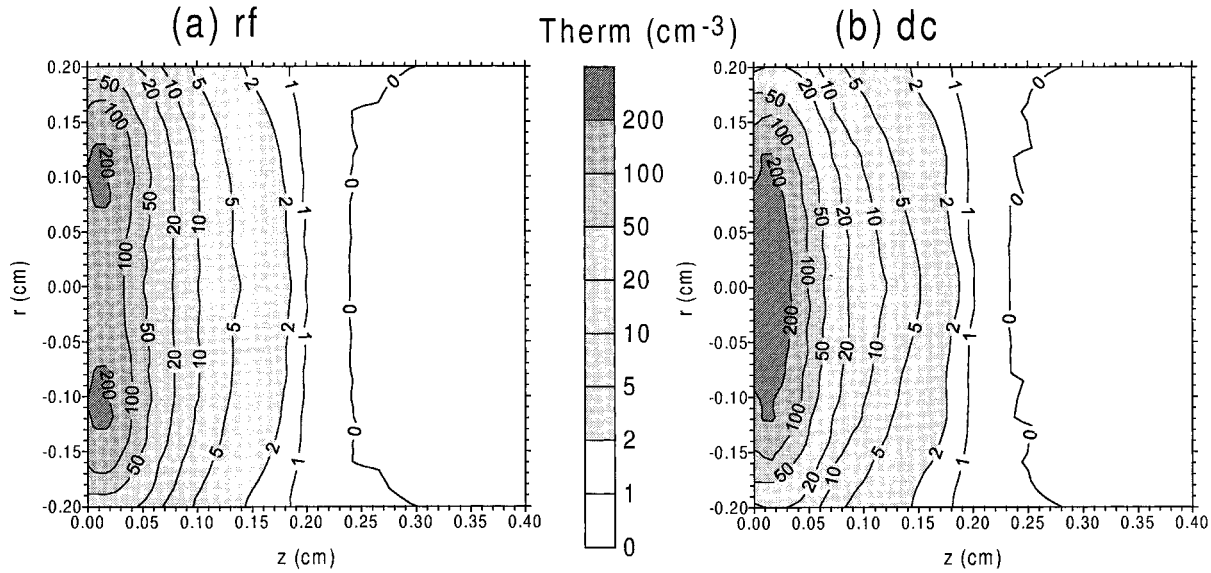

Fig. 6. Calculated two-dimensional thermalization profiles of the copper atoms, as number of atoms thermalized per cm^3, normalized to one sputtered atom, (a) in the rf discharge (constant in time) and (b) in the dc discharge, for the same conditions as in Fig. 3. Only the first 4 mm from the rf-electrode cathode are shown.

argon atoms play the dominant role in the sputtering process, both in the rf and dc mode, with a relative contribution of 69.5% (rf) and 68.8% (dc). However, since the bombarding energy is also important to determine the amount of sputtering, the argon and copper ions play also a non-negligible role in the sputtering process, in spite of their lower fluxes. Their contributions were calculated to be approximately 18.3% (rf) and 19% (dc) for the argon ions, and approximately 12.2% in both operation modes for the copper ions (called 'self-sputtering').

3.3. Thermalization profiles

Fig. 6 shows the calculated two-dimensional thermalization profiles of the sputtered copper atoms, both in the rf discharge (found to be constant in time) and in the dc discharge. Only the first 4 mm from the rf-electrode cathode are represented, because nearly all atoms are thermalized in this region. It is clear that most sputtered atoms become thermalized very close to the electrode (in the order of fractions of 1 mm), and only a very small fraction will become thermalized at distances further than 1–2 mm from the electrode. The thermalization profiles look very similar for both the rf and dc mode. These thermalization profiles are used as input values for the further calculation of the behavior of the copper atoms.

3.4. Le el populations

The calculated two-dimensional density profiles of the thermalized sputtered copper atoms in the ground level are illustrated in Fig. 7, both in the rf discharge (again found to be constant in time) and in the dc discharge. Again only the first 4 mm adjacent to the electrode are shown, because the distances further away from the electrode do not give additional information. In both cases, the density reaches a maximum of approximately 5 10^{14} cm ^{3} at less than 0.5 mm from the electrode. The maximum density in the dc case seems to be slightly higher than in the rf case, which is quite unexpected since the erosion rate was found to be slightly lower. However, as will be shown later, the level populations of excited copper atoms are somewhat higher in the rf case compared to the dc case, and moreover, the density profile of the rf copper atom ground state drops off more slowly than the corresponding dc density. In general, both density profiles look very similar to each other.

Fig. 8 depicts the calculated two-dimensional

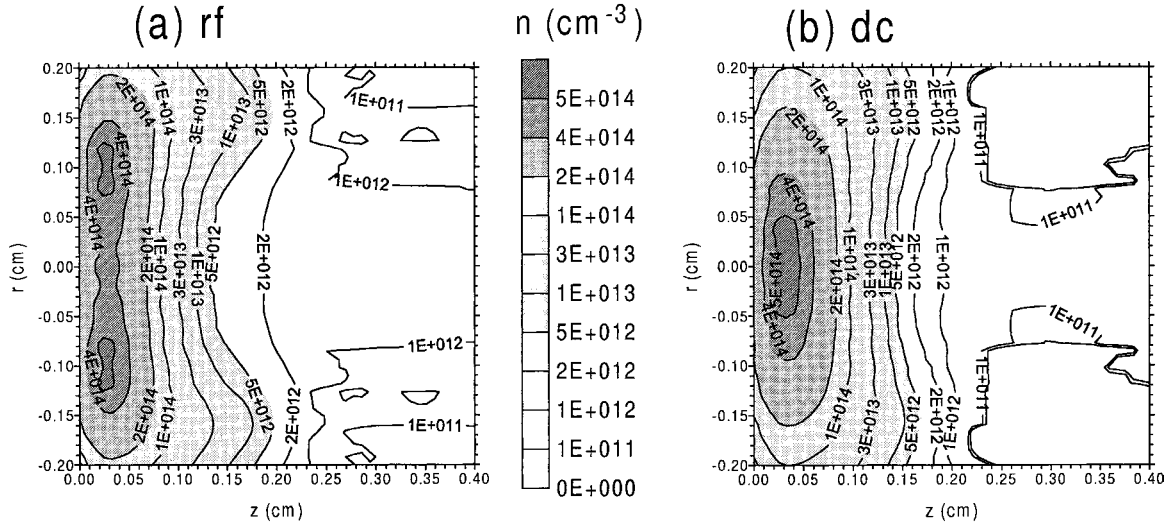

Fig. 7. Calculated two-dimensional density profiles of the thermalized copper atoms, (a) in the rf discharge (constant in time) and (b) in the dc discharge, for the same conditions as in Fig. 3. Only the first 4 mm from the rf-electrode cathode are shown.

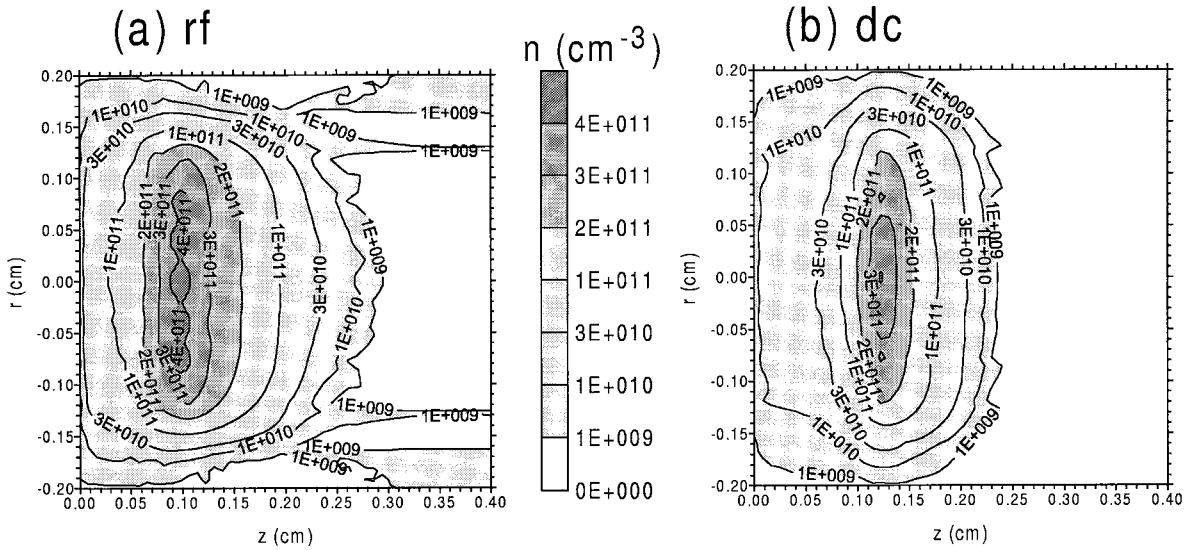

Fig. 8. Calculated two-dimensional density profiles of the Cu ions, (a) in the rf discharge (constant in time) and (b) in the dc discharge, for the same conditions as in Fig. 3. Only the first 4 mm from the rf-electrode cathode are shown.

density profiles of the Cu ions in the ground level, both in the rf discharge (again found to be constant in time) and in the dc discharge. The maximum densities are in the order of 4 10^{11} cm ^{3} at approximately 1 mm from the electrode and are again quite similar for both the rf and dc case. The dc Cu ion density reaches its maximum a little bit further away from the cathode and decreases more rapidly to lower values at the cathode compared to the rf density, due to the somewhat longer length of the dc cathode fall sheath (i.e. approx. 0.7 mm) compared to the rf sheath (i.e. varying between 0 and 0.6 mm). Nevertheless, the overall outlook of both the rf and

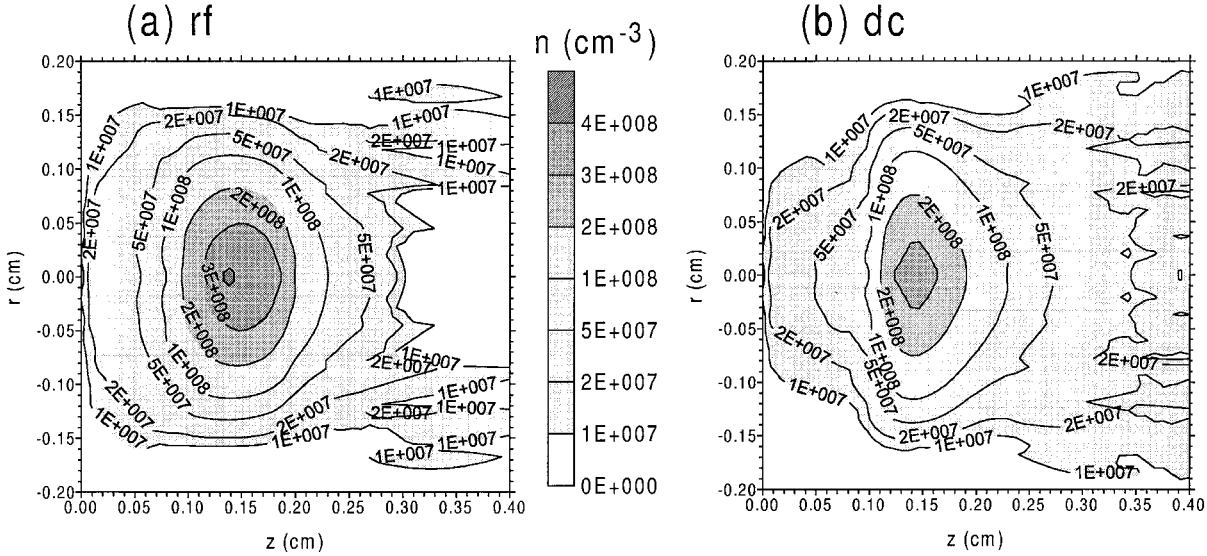

Fig. 9. Calculated two-dimensional density profiles of the Cu^{2} ions, (a) in the rf discharge (constant in time) and (b) in the dc discharge, for the same conditions as in Fig. 3. Only the first 4 mm from the rf-electrode cathode are shown.

dc Cu ion densities is again very similar. By comparing the absolute values of the Cu ion densities at their maximum with the copper atom maximum density values, the ionization degree could be estimated. It was found to be in the order of 0.1%, for both the rf and dc case.

The two-dimensional Cu^2 ion density profiles calculated for both the rf and the dc case, are presented in Fig. 9. Again the absolute values of the densities (i.e. maximum of approx. 3–4 10^8 cm ^{3}) and the relative shapes are nearly identical for both operation modes. Comparing the absolute values of Fig. 9 with those of Fig. 8 gives us the estimated ionization degree of Cu to Cu^2 . It was found to be also in the order of 0.1%, hence similar to the Cu^0–Cu ionization degree.

Since the two-dimensional density profiles of the excited copper atoms and ions look very similar to the ground state copper atom and ion density profiles, respectively, there is no need to illustrate the two-dimensional level population profiles of all excited levels here. However, Fig. 10 plots the level populations at the maximum of their profiles, divided by their statistical weights, against the level number i, for both the rf case (at four times in the rf-cycle, but the values are almost identical to each other; black lines) and the dc case (gray lines). It should indeed be mentioned that the populations are divided by the statistical weight, in order to account for variations in level populations, simply as a result of variations in statistical weights. It follows that the excited copper atomic levels are systematically a bit lower in the dc mode than in the rf mode. However, the copper ionic levels are characterized by similar level populations in both operation modes. Furthermore, it is seen that the populations of the excited levels generally decrease with increasing level number, and hence increasing excitation energy (see right axis, dashed line), which is quite logical. However, the excited levels were found to be not completely Boltzmann distributed (see also Bogaerts et al. 4), due to overpopulations of metastable levels and rather strong variations in excitation cross sections. Finally, the variations of rf and dc populations as a function of level number are found to be identical to each other.

3.5. Relati e contributions of arious populating and depopulating processes

Table 1 gives an overview of the relative contributions of the most important production and loss processes for several levels, in the rf discharge (at four times in the rf-cycle) and in the dc discharge. As mentioned before, the copper ground state atoms (i 1) are almost exclusively

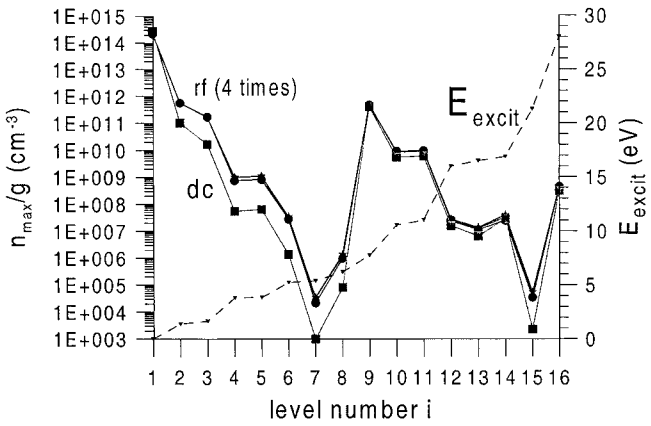

Fig. 10. Calculated level populations at the maximum of their profiles, divided by their statistical weights, as a function of the effective level number i, for the same conditions as in Fig. 3. The black lines represent the values in the rf discharge (at four times in the rf-cycle), and the gray lines indicate the dc values. Also shown in the figure are the excitation energies of the excited levels (dashed line, right axis).

Table 1
Relative contributions in (%) of the production and loss processes for the various levels

Level	Process	rf: π 2	rf: π	rf: 3π 2	rf: 2π	dc
i 1: Cu^0 $3d^{10}4s$	Production processes:					
	Sputtering	99.9	99.9	99.9	99.9	100
	Electron impact de-excitation from $3d^94s^2$ (metast)	0.1	0.1	0.1	0.1	0.03
	Loss processes:					
	Penning ionization	17.9	16.3	20.8	20.2	16.2
	Electron impact ionization	12.0	10.4	7.7	8.2	10.8
	Asymmetric charge transfer	0.1	0.1	0.1	0.1	0.1
	Electron impact excitation to $3d^94s^2$	10.9	12.9	15.8	14.3	12.8
	Electron impact excitation to $3d^{10}4p$	52.2	53.4	49.5	50.0	53.2
	Electron impact excitation to $3d^{10}4s4p$	2.2	2.4	2.2	3.1	2.3
	Electron impact excitation to $3d^{10}5p$ 4d	4.7	4.5	3.9	4.0	4.6
i 2: Cu^0 $3d^9$ $4s^2$	Production processes:					
	Electron impact excitation from Cu^0 ground state	80.1	79.4	76.9	80.3	91.9
	Electron impact de-excitation from higher $3d^94s^2$	19.8	20.6	23.0	19.6	8.1
	Loss processes:					
	Electron impact excitation to higher $3d^94s^2$	72.1	71.6	69.1	69.9	71.0
	Electron impact excitation to $3d^{10}4p$	2.0	2.0	2.1	2.0	2.0
	Electron impact excitation to $3d^{10}4s4p$	16.5	16.6	16.4	16.5	16.1
	Electron impact excitation to $3d^{10}5s$	0.4	0.5	0.6	0.6	0.5
	Electron impact excitation to $3d^{10}5p$ and 4d	3.9	3.9	3.3	3.5	3.7
	Electron impact ionization	5.0	5.4	8.5	7.3	6.5
i 4: Cu^0 $3d^{10}4p$	Production processes:					
	Electron impact excitation from Cu^0 ground state	99.7	99.7	99.7	99.8	99.9
	Electron impact excitation from $3d^94s^2$	0.3	0.3	0.3	0.2	0.1
	Loss processes:					
	Radiative decay to Cu^0 ground state	51.7	51.6	48.8	45.9	60.9
	Radiative decay to $3d^94s^2$	27.7	27.2	24.8	26.1	21.7
	Electron impact excitation to higher levels	12.4	12.8	15.9	16.9	10.5
	Electron impact de-excitation to lower levels	4.2	4.0	4.3	4.9	2.9
	Electron impact ionization	4.0	4.4	6.1	6.2	3.8
i 6: Cu^0 $3d^94s4p$	Production processes:					
	Electron impact excitation from Cu^0 ground state	55.7	56.9	58.9	61.2	78.7
	Electron impact excitation from $3d^94s^2$	44.2	43.1	41.0	38.8	21.3
	Loss processes:					
	Radiative decay to Cu^0 ground state	47.6	47.3	45.9	42.4	52.7
	Radiative decay to $3d^94s^2$	35.0	35.3	32.6	34.7	31.1
	Electron impact ionization	10.2	11.0	16.0	16.2	11.0
	Electron impact de-excitation to lower levels (mainly $3d^94s^2$)	7.1	6.4	5.5	6.6	4.8

Table 1 (*Continued*)

Level	Process	rf: π 2	rf: π	rf: 3π 2	rf: 2π	dc
i 8: Cu^0 $3d^{10}$ 5p, 3d	Production processes:					
	Electron impact excitation from Cu^0 ground state	99.0	99.0	99.0	99.1	99.6
	Electron impact excitation from $3d^9 4s^2$	1.0	1.0	1.0	0.9	0.4
	Loss processes:					
	Radiative decay to Cu^0 ground state	2.5	2.5	2.6	2.4	3.1
	Radiative decay to $3d^9 4s^2$	11.0	11.0	10.9	10.8	10.9
	Radiative decay to $3d^{10} 4p$	74.9	75.0	74.3	73.9	74.3
	Radiative decay to $3d^{10} 5s$	4.7	4.7	4.7	4.7	4.7
	Electron impact ionization	3.1	3.0	3.4	3.7	3.1
	Electron impact de-excitation to lower levels (mainly $3d^{10} 5s$)	3.8	3.7	4.1	4.5	3.9
i 9: Cu $3d^{10}$ (ground state)	Production processes:					
	Penning ionization	64.4	62.4	51.5	51.7	51.0
	Electron impact ionization	35.4	37.4	48.2	48.0	48.6
	Radiative decay from Cu $3d^9 4p$	0.2	0.2	0.2	0.3	0.3
	Loss processes:					
	Electron impact excitation to Cu $3d^9 4s$	68.8	67.9	61.1	62.5	62.7
	Electron impact excitation to Cu $3d^9 4p$	30.8	31.8	38.2	36.9	36.7
	Electron impact ionization	0.3	0.3	0.7	0.6	0.5
i 10: Cu $3d^9 4s$	Production processes:					
	Penning ionization	81.7	81.2	70.1	73.6	73.6
	Electron impact ionization	12.6	13.3	24.9	20.6	20.0
	Radiative decay from Cu $3d^9 4p$	4.4	4.2	3.9	4.5	4.9
	Electron impact excitation from Cu ground	1.3	1.3	1.1	1.3	1.5
	Loss processes:					
	Electron impact excitation to Cu $3d^9 4p$	97.0	97.1	97.5	97.5	97.1
	Electron impact excitation to Cu $3d^9 5s$	2.6	2.6	2.0	2.0	2.4
	Electron impact ionization	0.3	0.3	0.5	0.5	0.5
i 12: Cu $3d^9$ 4p ($^3P_2$)	Production processes:					
	Asymmetric charge transfer	90.6	90.1	88.7	89.2	88.4
	Electron impact excitation from Cu ground	5.3	5.7	6.5	6.3	6.9
	Electron impact excitation from Cu $3d^9 4s$	4.0	4.2	4.7	4.4	4.6
	Radiative decay from Cu $3d^9 5s$	0.1	0.1	0.1	0.1	0.1
	Loss processes:					
	Radiative decay to Cu $3d^9 4s$	99.8	99.8	99.8	99.8	99.8
	Electron impact de-excitation to Cu $3d^9 4s$	0.1	0.1	0.1	0.1	0.1

Table 1 (*Continued*)

Level	Process	rf: π 2	rf: π	rf: 3π 2	rf: 2π	dc
i 13: Cu $3d^9 4p$	Production processes:					
(other)	Electron impact excitation from Cu ground	5.1	5.2	5.6	5.7	5.9
	Electron impact excitation from Cu $3d^9 4s$	94.8	94.6	94.3	94.2	94.0
	Radiative decay from Cu $3d^9 5s$	0.1	0.1	0.1	0.1	0.1
	Loss processes:					
	Radiative decay to Cu $3d^9 4s$	99.7	99.7	99.7	99.7	99.6
	Electron impact excitation to Cu $3d^9 5s$	0.1	0.1	0.1	0.1	0.1
	Electron impact de-excitation to Cu $3d^9 4s$	0.2	0.2	0.2	0.2	0.3
i 15: Cu $3d^9 5s$	Production processes:					
	Electron impact excitation from Cu $3d^9 4p$	100	100	100	100	100
	Loss processes:					
	Radiative decay to Cu $3d^9 4p$	99.5	99.5	99.5	99.5	99.4
	Electron impact de-excitation to Cu $3d^9 4p$	0.4	0.4	0.4	0.4	0.5
	Electron impact ionization	0.1	0.1	0.1	0.1	0.1
i 16: Cu^2	Production processes:					
	Electron impact ionization from Cu^0 ground	74.0	82.3	86.4	75.9	90.3
	Electron impact ionization from Cu ground	9.8	7.3	6.4	10.8	4.7
	Electron impact ionization from Cu $3d^9 4s$	15.8	10.2	7.0	12.9	4.9
	Electron impact ionization from Cu $3d^9 4p$	0.4	0.2	0.2	0.3	0.1
	Loss processes:					
	Electron–ion three-body recombination	100	100	100	100	100

formed by sputtering at the rf-electrode or cathode, both in the rf and dc discharge. The most important loss processes are electron impact excitation to higher levels (primarily to the $3d^{10}$ 4p levels and the $3d^9$ $4s^2$ levels), as well as electron impact ionization to Cu and Penning ionization by argon metastable atoms. The calculated relative contributions of the production and loss processes are very similar for the rf and dc mode, and do not vary significantly in time in the rf mode. It appears that asymmetric charge transfer with argon ions (i.e. Cu^0 Ar $\rightarrow$ Cu Ar^0) is only of minor importance as an ionization process, for the discharge conditions under investigation and the Grimm-type cell with 4-mm anode diameter. The reason is that the calculated copper atom density reaches a maximum very close to the electrode (see Fig. 7), and has dropped to low values at approximately 0.1 cm, where the argon ion density reaches its maximum (i.e. the argon ion density profile has a similar shape as the copper ion density profile, presented in Fig. 8). In previous calculations for an 8-mm anode Grimm-type cell 10 , the copper atom density reached its maximum at a distance further away from the cathode (since a smaller fraction of the copper atoms was lost due to diffusion to the side walls), and it showed a much better overlap with the argon ion density, leading to more asymmetric charge transfer. Experimentally, it was also demonstrated that this process is quite important at typical Grimm-type conditions 11 , but these measurements were also performed in an 8-mm anode source. Nevertheless, it is our feeling that the presently calculated role of asymmetric charge transfer is somewhat too low, possibly due to a too rapid drop of the sputtered copper atom density. In future work, we would like to test this in more detail, e.g. by comparison of calculated and experimental emission intensities (see below).

Furthermore, in Table 1, it follows that the Cu^0 $3d^9 4s^2$ (metastable) levels (*i* 2 and 3) and the

Cu^0 $3d^{10}4p$ levels (i 4 and 5) are mainly formed by direct electron impact excitation from the Cu^0 ground state. It is worth mentioning that these levels are very important in copper vapor lasers. Indeed, lasing lines are observed between the Cu^0 $3d^{10}4p$ levels (as upper levels) and the Cu^0 $3d^94s^2$ levels (as lower levels) 12 . Collisional mixing within the two $3d^94s^2$ levels and the two $3d^{10}4p$ levels is quite important. For the $3d^{10}4p$ levels it is not explicitly considered in the model, because these levels are lying so close to each other that excitation and de-excitation are equally important and the levels are actually populated according to their statistical weights. For the $3d^94s^2$ levels, which are lying somewhat more separated from each other, excitation and de-excitation by electron, argon or copper atom impact are explicitly taken into account. Indeed, it appears from Table 1 that electron impact de-excitation from the higher $3d^94s^2$ level is a rather important production process for the lower $3d^94s^2$ level (i 2), and especially electron impact excitation to this higher $3d^94s^2$ level is a dominant loss process. Beside that, also electron impact excitation to higher Cu^0 excited levels, as well as electron impact ionization are quite significant loss processes for the $3d^94s^2$ levels. Collisional mixing between these levels due to argon or copper atom impact, on the other hand, is actually found to be negligible, both as production and loss process for these levels. Moreover, since the $3d^94s^2$ levels are metastable, they cannot be depopulated by radiative decay. This is certainly not the case for the $3d^{10}4p$ levels, which are very efficiently depopulated by radiative decay, both to the Cu^0 ground state (giving rise to the so-called resonant lines at 324.7 and 327.4 nm) and to the $3d^94s^2$ metastable levels (which can result in laser lines, for appropriate conditions like in copper vapor lasers, see above). Furthermore, electron impact de-excitation to the lower levels and electron impact ionization play also some role in depopulating these $3d^{10}4p$ levels. Again, no significant differences are observed between the rf and dc mode, and as a function of time in the rf-cycle.

The higher Cu^0 excited levels (e.g. $3d^94s4p$: i 6; and $3d^{10}$ 5p and 3d: i 8) are also mainly populated by direct electron impact excitation from the Cu^0 ground state, although for the $3d^94s4p$ levels stepwise excitation from the $3d^94s^2$ metastable levels is also quite important. The levels are predominantly lost by radiative decay to lower levels, although electron impact de-excitation to the lower levels and electron impact ionization also play a non-negligible role. Again, there are no major differences between both operation modes, and no significant variations as a function of time.

The Cu $3d^{10}$ ground level (i 9) and the Cu $3d^94s$ metastable levels (i 10 and 11) are mainly populated by Penning ionization and electron impact ionization from the Cu^0 ground state and excited levels. Indeed, it is assumed in our model that these two ionization processes can only lead to the formation of the Cu ground state or metastable levels, and not to Cu higher excited levels. A detailed justification of this assumption can be found in Bogaerts et al. 4 . Depopulation of these levels occurs mainly by electron impact excitation to the higher Cu levels (i.e. mainly to the $3d^94s$ and $3d^94p$ levels for the Cu ground state, and to the $3d^94p$ levels for the Cu metastable levels).

The $3d^94p$ levels (i 12, 13 and 14) are predominantly populated by electron impact excitation from the Cu metastable levels, and to a less extent from the Cu ground state. However, the $3d^94p$ ($^3P_2$) level (i 12) forms an exception to this, because it is mainly populated by asymmetric charge transfer between Cu^0 ground state atoms and Ar ions. This is the reason why this level is not included in the effective level i 13, but is treated as a separate, individual level. Indeed, the Ar ions show only good energy overlap with this Cu $3d^94p$ $^3P_2$ energy level, so that it is assumed that asymmetric charge transfer selectively populates only this level. This is in correspondence with the experimental observations of Steers et al. 11 , who found that the emission lines originating from this Cu level were systematically higher, due to selective population of this level. The loss of all $3d^94p$ levels occurs almost entirely by radiative decay to the $3d^94s$ levels, as appears from Table 1.

The highest Cu levels taken into account in our model, i.e. the $3d^95s$ levels (i 15) are exclu-

sively formed by electron impact excitation from the Cu $3d^9 4p$ levels, and the dominant loss mechanism is found to be radiative decay to these levels.

Finally, the Cu^2 ions seem to be primarily created by electron impact ionization from the Cu^0 ground state (i.e. the removal of two electrons at the same time), although electron impact ionization from the Cu ground state and metastable levels also contribute for approximately 5–15% each. Indeed, although the cross section for double electron impact ionization (i.e. from Cu^0 to Cu^2) is clearly lower than the electron impact ionization cross section from Cu to Cu^2 (see ref. 4), the first process is still more important, due to the much higher density of Cu^0 atoms compared to Cu ions. The loss of the Cu^2 ions appears to be caused for 100% by electron–ion three-body recombination, which is logical because this was the only loss mechanism for Cu^2 ions taken into account in our model. In analogy to the copper atomic levels, the relative contributions of the various populating and depopulating processes for the Cu levels and

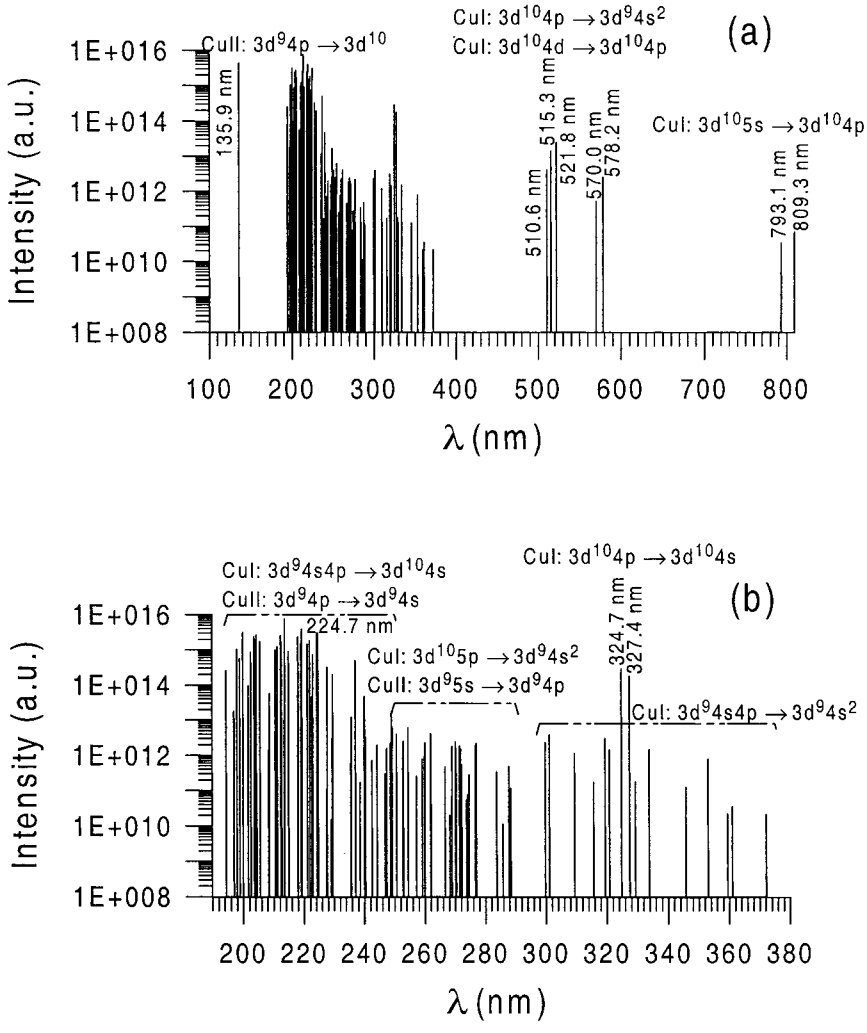

Fig. 11. Calculated optical emission spectrum in the rf discharge (more or less constant in time). Both (a) the entire spectral range and (b) a detail (190–380 nm) are shown.

the Cu^2 ions do not vary significantly in time and are rather similar for both the rf and dc operation modes.

3.6. Optical emission intensities

From the level populations of the excited copper atomic and ionic levels, the optical emission intensities of spectral lines can be calculated, when multiplying these populations with the Einstein transition probabilities for radiative decay. Fig. 11 shows the calculated optical emission spectrum in the rf discharge (found to be constant in time, since the level populations were also constant, see Fig. 10). Both the entire spectral range and, in more detail, the 190–380-nm range, where most lines are present, are shown. Similar spectra are shown in Fig. 12 for the dc discharge. In general it appears that the dc optical emission intensities are somewhat lower than the corresponding rf intensities. This seems to be especially the case for the atomic lines (i.e. the dc values were found to be approximately one order of magnitude lower), whereas the ionic lines

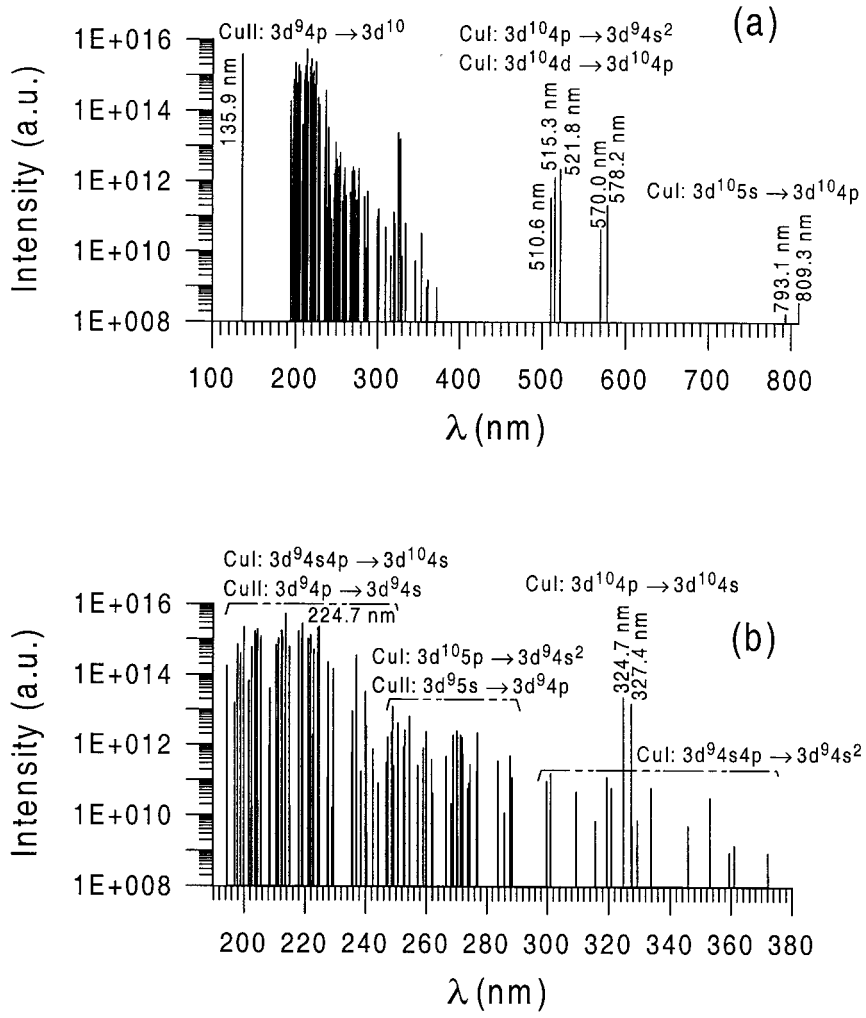

Fig. 12. Calculated optical emission spectrum in the dc discharge. Both (a) the entire spectral range and (b) the 190–380 nm range are shown.

showed only a difference of 10–20%. Indeed, Fig. 10 revealed also that the dc atomic level populations were clearly lower than the rf values, whereas the ionic levels were almost of the same magnitude. Experimentally, the Cu intensities were found to be approximately 10% lower in the dc case compared to the rf case. Hence, this is apparently in good agreement with our calculated differences for the ionic lines, but the differences we calculated for the atomic lines seem to be somewhat too high. In general, both the rf and the dc spectra have a very similar outlook.

It is also interesting to mention that the ionic lines were found to be more intense than the atomic lines, even than the two resonant lines (i.e. 324.7 nm and 327.4 nm). The reason for this is the rather strong self-absorption of these resonant lines in the model. Whether this behavior of more intense ionic than atomic lines is also experimentally the case needs to be further investigated. Finally, it should be mentioned that the 224.7 nm line, which corresponds to a $3d^9$ 4p $^3P_2$–$3d^9$ 4s transition, although having a very high intensity, is not the dominant line in the spectrum. Steers and coworkers, on the other hand, clearly observed this as the most intense line in the spectrum [11], and attributed this to selective excitation by asymmetric charge transfer of the upper level (see above). In a previous paper [13], where the Grimm-type source of 8-mm anode diameter was investigated, we also predicted that this line dominated the spectrum, because asymmetric charge transfer appeared to be much more important. However, as mentioned before, it might well be that this process is underestimated in the model at the present discharge conditions, and that the intensity of the 224.7-nm line should be higher in the spectrum. Therefore, in the near future, we would like to compare the calculated rf and dc spectra in more detail with experimental observations.

4. Conclusion

A number of models has been developed, describing the behavior of the copper species in rf and dc glow discharges. They allow the calculation of, among others, sputtering rates, level populations of various copper atomic and ionic levels, and optical emission intensities of lines emitted by excited copper atoms and ions. The sputtering is calculated from an empirical formula for the sputtering yield multiplied with the flux energy distributions of the bombarding species. The thermalization process after sputtering is treated with a Monte Carlo model. The further behavior of the copper atoms, the ionization and excitation, and the behavior of the excited copper atomic and ionic levels, are handled in a collisional–radiative model. Finally, the transport of the copper ions in the sheath is also simulated with a Monte Carlo method. These models are coupled to the other models we have developed previously for the other plasma species, and solved iteratively until final convergence is reached. The model is applied to a simplification of the Grimm-type cell, and is run for typical operating conditions: 5 torr gas pressure, 37–38 W electrical power, a dc voltage of 1000 V, or rf voltages of 769 V (rf amplitude) and 519 V (dc bias). These calculated electrical parameters are in reasonable agreement with experimental values measured by Hoffmann.

The calculated erosion rates, at the same values of gas pressure and electrical power, are found to be slightly higher in the rf mode than in the dc mode, which is also found experimentally. The absolute values of the calculated erosion rates are in reasonable agreement with experimental observations for the same discharge conditions.

The calculated thermalization profiles, as well as the density profiles of the thermalized copper atoms, reach a maximum very close to the rf-electrode cathode, and are nearly identical in both operation modes, both in absolute values and in relative shapes. The latter is also true for the calculated density profiles of the Cu and Cu^2 ions. By comparing the values at the maximum of their profiles for all copper atomic and ionic levels, it follows that the calculated copper atom excited level populations are systematically lower in the dc case compared to the rf case. The

excited ionic levels, on the other hand, were found to have more or less the same populations in both operation modes.

Concerning the relative contributions of populating and depopulating processes, it is found that electron impact excitation from the ground state, but also from excited levels, is the most important production process for all levels, either atomic or ionic. Only for the Cu ground state and $3d^9 4s$ metastable levels, the dominant production mechanism is Penning ionization and electron impact ionization, and the Cu $3d^9 4p\ ^3P_2$ level is predominantly created by asymmetric charge transfer. The Cu^0 and Cu ground states and metastable levels are mainly depopulated by electron impact excitation to higher levels and to a less extent by electron impact ionization, whereas the most important loss mechanism for the other atomic and ionic excited levels is radiative decay to the lower levels. The relative contributions of the various populating and depopulating processes were found not to vary significantly in time, and to be more or less similar for both the dc and the rf operation modes.

Finally, the optical emission spectra were calculated for both rf and dc mode. The spectra look qualitatively very similar, however the dc intensities were found to be lower than the rf intensities, i.e. approximately an order of magnitude for the atomic lines, but only 10–20% for the ionic lines. Experimentally, the dc intensities were also found to be lower by approximately 10%. In the near future, we plan to compare the calculated spectra for both operation modes in more detail with experimentally measured spectra.

Acknowledgements

A. Bogaerts is indebted to the Flemish Fund for Scientific Research (FWO) for financial support. This research is also sponsored by the Federal Services for Scientific, Technical and Cultural Affairs of the Prime Minister's Office (DWTC SSTC) through IUAP-IV (Conv. P4 10). Finally, we wish to thank V. Hoffmann for supplying the experimental data.

References

1 A. Bogaerts, R. Gijbels, Description of the argon-excited levels in a radio-frequency and direct current glow discharge, Spectrochim. Acta Part B 55 (2000) 263.
2 A. Bogaerts, R. Gijbels, J. Appl. Phys. 79 (1996) 1279.
3 A. Bogaerts, M. van Straaten, R. Gijbels, J. Appl. Phys. 77 (1995) 1868.
4 A. Bogaerts, R. Gijbels, R.J. Carman, Spectrochim. Acta Part B 53 (1998) 1679.
5 V. Hoffmann, private communication.
6 A. Bogaerts, R. Gijbels, W.J. Goedheer, Spectrochim. Acta Part B 54 (1999) 1335.
7 N. Matsunami, Y. Yamamura, Y. Itikawa, N. Itoh, Y. Kazumata, S. Miyagawa, K. Morita, R. Shimizu, T. Tawara, At. Data Nucl. Data Tables 31 (1984) 1.
8 A. Bogaerts, R. Gijbels, Spectrochim. Acta Part B 52 (1997) 765.
9 R.C. Weast, M.J. Astle, CRC Handbook of Chemistry and Physics, 63rd ed, CRC Press, Boca Raton, FL, 1982 1983.
10 A. Bogaerts, R. Gijbels, Spectrochim. Acta Part B 53 (1998) 437.
11 E.B.M. Steers, R.J. Fielding, J. Anal. At. Spectrom. 2 (1987) 239.
12 R.J. Carman, D.J.W. Brown, J.A. Piper, IEEE J. Quant. Electron. 30 (1994) 1876.
13 A. Bogaerts, R. Gijbels, J. Anal. At. Spectrom. 13 (1998) 721.